



## Science Arts & Métiers (SAM)

is an open access repository that collects the work of Arts et Métiers ParisTech researchers and makes it freely available over the web where possible.

This is an author-deposited version published in: <http://sam.ensam.eu>  
Handle ID: <http://hdl.handle.net/10985/8549>

### To cite this version :

Thanh Hung NGUYEN, Christophe GIRAUD-AUDINE, Betty LEMAIRE-SEMAIL, Gabriel ABBA, Régis BIGOT - Modelling of piezoelectric actuators used in forging processes: principles and experimental validation - In: Electrical Machines (ICEM), 2012 XXth International Conference on, France, 2012-09-02 - XX international Conference on Electrical Machines (ICEM) - 2012

Any correspondence concerning this service should be sent to the repository

Administrator : [archiveouverte@ensam.eu](mailto:archiveouverte@ensam.eu)

# Modelling of piezoelectric actuators used in forging processes: principles and experimental validation

T. H. Nguyen, C. Giraud-Audine, B. Lemaire-Semail, G. Abba, R. Bigot

**Abstract**—This paper deals with the modelling of a piezoelectric stack actuator used to generate specific low frequency vibration waveforms to assist forging processes. Experimental results show that such waveforms reduce the necessary forging force during upsetting tests. The main problems which remain are defining the appropriate waveforms, predicting their influence on the process and the actuator and designing the control. Due to the complexity of the interactions between the different components of the system, a complete model of the process is needed. Such a model is developed here using an energetic macroscopic representation to preserve causality throughout the modelling. Simulation results are then compared to representative experimental results.

**Index Terms**—Energetic Macroscopic Representation, Forging, Graphical models, Modelling, Piezoelectric actuator

## I. NOMENCLATURE

Displacement	$q$	[m]
Force generated by PA	$F$	[N]
Piezoelectric force	$F_C$	[N]
Elastic force	$F_S$	[N]
Forging load	$F_M$	[N]
Electrical charge	$Q$	[C]
Voltage	$U$	[V]
Current entering the actuator	$i$	[A]
Motional current	$i_C$	[A]
Stiffness of PA	$K_S$	$[\frac{N}{m}]$
Electromechanical conversion factor	$K_C$	$[\frac{C}{m}]$
Electrical capacitor of PA	$C$	[F]
External radius of workpiece	$r_e$	[m]
Height of workpiece	$h$	[m]
Coulomb coefficient	$\mu$	[-]
Flow stress	$\sigma_0$	[Pa]
Material yield stress	$\sigma_y$	[Pa]
Hardening stress	$\sigma_H$	[Pa]
Viscous stress	$\sigma_v$	[Pa]
Material strain	$\varepsilon$	[-]
Material strain in plastic domain	$\varepsilon_p$	[-]
Material strain in elastic domain	$\varepsilon_e$	[-]
Young's modulus	$E$	[Pa]
Hardening modulus	$H$	[Pa]
Dynamical viscous coefficient	$\eta$	[Pa.s]

T. H. Nguyen, Ch. Giraud-Audine, B. Lemaire-Semail are with Laboratoire d'Electrotechnique et d'Electronique de Puissance de Lille (L2EP), Universit des Sciences et Technologies de Lille (USTL), Villeneuve d'Ascq, France (email: thanh-hung.nguyen@ensam.eu)

G. Abba, R. Bigot are with Laboratoire de Conception, Fabrication et Commande (LCFC), École Nationale Supérieure d'Arts et Métiers de Metz, Metz, France (email: gabriel.abba@ensam.eu)

## II. INTRODUCTION

The advantages of using vibrations to reduce the required force and improve the quality of the finished product in the forming process are currently being studied by different researchers. Ultrasonic sinusoidal mechanical vibrations are applied in the works as to the tooling during extrusion [?], drawing [?] or compression tests [?]. It has been reported that the mean force is reduced. Fig.1 presents the seminal result obtained by Blaha [?] in which vibrations of 10-15 kHz were superimposed during a tensile test, which caused a reduction of the applied force to a zinc specimen. Langevin resonators were used to apply these vibrations.

Recent results seem to indicate that low frequency waveforms can have a similar effect. This observation is important as it means that a wider range of waveforms can be used, waveforms produced by the piezoelectric actuators (PA). Indeed, piezostack actuators are a compromising source of vibrations to assist the forming process, especially forging processes (FP), because of their high stiffness and the high levels of force they generate compared to their compact size.

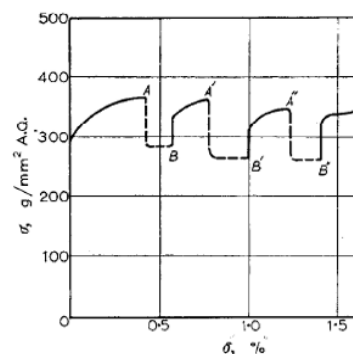


Fig. 1. Stress-strain curve of zinc crystals under ultrasonic action [?]

However, the load is very non-linear due to the plastic behaviour of the workpiece. Therefore, there is a need for simulation in order to:

- Evaluate the effects of a specific waveform on the forging force,
- Study the perturbation of the load on the actuator,
- Design the control for the process,
- Predict the interaction with the power supply.

In this paper, a model of complete forging process using the assistance of vibration will be established to study the effect of low frequency waveform on the process. In the first part, the modelling principles will be explained and then applied to the different parts of the system. The second part gives a short introduction to the experimental apparatus used

in this work, then focuses on simulation results and their validation compared to experimental results.

### III. MODELLING

#### A. Introduction

The process studied is the upsetting of a cylindrical workpiece (see Fig.2). Supposing that the upper and lower dies are rigid, the height  $h(t)$  is imposed on the workpiece by their relative motions. The upper die is assumed to move down at constant speed, while the lower die is animated by periodic vibration due to the PA. During the process, the workpiece reaction  $F_M$  is transmitted to the dies. The objective of this section is to model this whole system in order to study the feasibility of using the waveforms and to evaluate their influence on  $F_M$ .

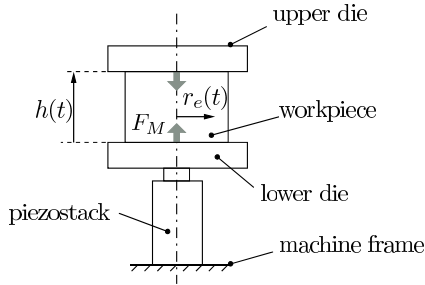


Fig. 2. Schematic of vibration assistance during upsetting of a cylindrical sample

In order to carry out the modelling, the Energetic Macroscopic Representation (EMR) [?] developed by the Laboratory of Electrical Engineering and Power Electronics (L2EP-France) is a helpful tool for visualizing causality and clearly understanding the power flows inside the system. Moreover, it gives an easy and solid method of designing the control. EMR takes no assumptions from mathematical systems into account but concentrates solely on power conversion by using a limited set of symbolic representations (power sources, storage, conversion and coupling, presented in Appendix VI) to highlight the system's energetic properties. Since the nature of each block imposes what can be applied (action) and how the block responds (reaction), causality is revealed naturally throughout the modelling process.

The symbolic representations of the piezoelectric actuator and workpiece presented in Fig.2 are described below.

#### B. Energetic Macroscopic Representation of a piezoelectric actuator

At this stage of the study, a sophisticated model of the piezoelectric is not required. The quasi-static equations widely used by most commercial PA suppliers are:

$$Q = K_C \cdot q + C \cdot U \quad (1)$$

$$F = K_S \cdot q + K_C \cdot U \quad (2)$$

Considering these equations from the view of physical quantity causality, they can be rewritten in the following natural integral causal forms:

$$\int i dt = K_C \cdot \int \dot{q} dt + C \cdot U \quad (3)$$

$$F = K_S \cdot \int \dot{q} dt + K_C \cdot U \quad (4)$$

Using the EMR symbols given in Appendix VI, the EMR model of the PA will be constructed step by step from the starting point of the entering variables and exiting variables. Following equations (3) and (4), we must obviously use the current and displacement as the entering variables in the EMR model. These quantities are accumulated inside the PA in the form of electrical and mechanical energy, which are represented by the accumulators (see Fig.3). The accumulators' outputs are expressed by the causality principle:

$$U = \frac{1}{C} \int (i - i_C) dt \quad (5)$$

$$F_S = K_S \int \dot{q} dt \quad (6)$$

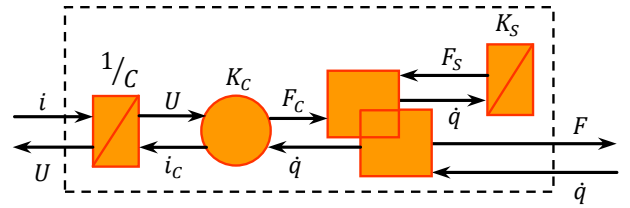


Fig. 3. EMR model for a piezoelectric actuator in the quasi-static mode

Next, the piezoelectric phenomenon is illustrated by a conversion element (the round one) with a conversion factor  $K_C$ . The relations between the inputs and outputs are defined by the following equations:

$$F_C = K_C \cdot U \quad (7)$$

$$i_C = K_C \cdot \dot{q} \quad (8)$$

where  $i_C$  is the motional current, and  $F_C$  is the piezoelectric force. The mechanical energy generated from the electromechanical conversion, defined by  $\int F_C \dot{q} dt$ , is stored partly in the mechanical accumulator, defined by  $\int F_S \dot{q} dt$ , and results partly in the output force  $F$ , defined by  $\int F \dot{q} dt$ . Therefore, this energetic relation can be determined by a coupling element and these forces are related by the following equation:

$$F_C = F_S + F \quad (9)$$

#### C. Modelling of cylindrical workpiece

The objective of this model is to determine the forging load during the FP. This is achieved using the slab method [?]. Assuming that the material flows radially, the resulting stress field depends solely on the current radius.

In this model, friction is taken into account using the Coulomb model and the sample's geometry is assumed to be conserved during the FP, which means that our sample will retain its cylindrical form. It also means that when the displacement is imposed on the sample by the rigid die, the sliding phenomenon will occur right at the interface during deformation. Writing the equilibrium of slab, the forging load can be obtained by the following equation:

$$F_{fp} = \frac{\pi r_e h}{\mu} \sigma_0 \left( \frac{e^A - 1}{A} - 1 \right) \quad (10)$$

where we introduce  $A = \frac{2\mu r_e}{h}$ . Rewriting this equation as:

$$F_{fp}(t) = \Psi(h(t)) \sigma_0[\varepsilon(t), \dot{\varepsilon}(t)] \quad (11)$$

reveals that the forging load is equal to the material's flow stress  $\sigma_0$  modulated by the function  $\varepsilon(t) = \frac{\pi r_e h}{\mu} \left( \frac{e^A - 1}{A} - 1 \right)$ , which depends on the Coulomb friction coefficient  $\mu$  and the geometric parameters of the workpiece  $h(t)$  and  $r_e(t)$ . The latter are imposed by the distance separating the dies  $h(t)$  (see Fig.2) and the volume conservation of the workpiece. Therefore, in order to calculate the reaction force, it is essential to estimate the current stress of the cylinder during the FP. This can be accomplished by introducing the constitutive law of the material which relates the flow stress's value to the strain and the strain rate, which are already functions of time:

$$\sigma_0(t) = \sigma_0[\varepsilon, \dot{\varepsilon}] \quad (12)$$

where  $\varepsilon(t)$  and  $\dot{\varepsilon}(t)$  are imposed by the distance between the dies  $h(t)$  [?]:

$$\begin{cases} \varepsilon(t) = 1 - \frac{h_0}{h(t)} \\ \dot{\varepsilon}(t) = \frac{d\varepsilon(t)}{dt} \end{cases} \quad (13)$$

Different analytical models can be applied to describe the behaviour of material during the forming process. In the present work, a uni-axial Bingham generalized elasto-viscoplastic model (Fig.4) is applied, as it describes the material behaviours both in the elastic and viscoplastic domains. This is obtained by introducing a slider which imposes  $\dot{\varepsilon}(t) = 0$  as long as  $|\sigma_0(t)| \leq \sigma_y$  where  $\sigma_y$  is the yield stress of the material. In such a case, the material is in the elastic domain and thus behaves like a spring with stiffness  $E$ . Otherwise, plastic flow occurs, and the slider imposes the stress  $\sigma_y$ . The material reacts like a system including a spring in parallel with a viscous damper of damping coefficient  $\eta$  submitted to stress  $\sigma_0(t) - \sigma_y$ .

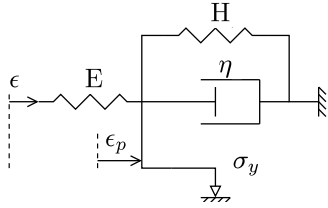


Fig. 4. Bingham's generalized analytical elasto-viscoplastic model

The model's input is the material strain, which is the sum of the elastic strain and the plastic strain:

$$\varepsilon(t) = \varepsilon_p(t) + \varepsilon_e(t) \quad (14)$$

The two states can be discriminated with the help of a control function:

- 1)  $|E \cdot \varepsilon - \sigma_H| < \sigma_y$ : elastic domain which corresponds to the EMR in Fig. 5a, where  $\varepsilon_p = 0$  (no plastic flow),
- 2)  $|E \cdot \varepsilon - \sigma_H| > \sigma_y$ : plastic domain, in which the plastic flow appears and the plastic stress  $\sigma_v$  can be determined by:

$$\begin{cases} \sigma_v = \sigma_0 - \sigma_H - \sigma_y & \text{if } E \cdot \varepsilon - \sigma_H > \sigma_y \\ \sigma_v = \sigma_0 - \sigma_H + \sigma_y & \text{if } E \cdot \varepsilon - \sigma_H < -\sigma_y \end{cases} \quad (15)$$

and in this case, the corresponding EMR is presented in Fig.5b.

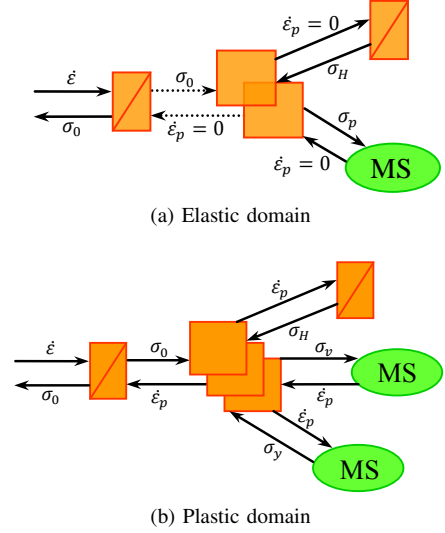


Fig. 5. Material behaviour's EMR

Note that in the current implementation, the non-linear elements for hardening stress and viscous stress were used, namely:

$$\begin{cases} \sigma_v = \eta |\dot{\varepsilon}_p|^n \text{sgn}(\dot{\varepsilon}_p) \\ \sigma_H = H |\varepsilon_p|^m \text{sgn}(\varepsilon_p) \end{cases} \quad (m, n > 0) \quad (16)$$

where  $\text{sgn}(\cdot)$  is the sign function.

Parameters  $E, H, \sigma_y, m, n$  are assumed to be constant for a specific material. The solution of equation (15) returns the value of plastic strain  $\varepsilon_p$  as a function of the input  $\varepsilon$ . The elastic strain  $\varepsilon_e$  can then be deduced according to (14).

Finally, the two models described are connected to the model of the mechanical system including the lower die and the elastic links (described in the next section) to create a complete model (Fig.6) for the experimental system. Note that the upper die is supposed to be in contact with the workpiece continuously. However, it is the case in practice since the vibrations' amplitude is very small.

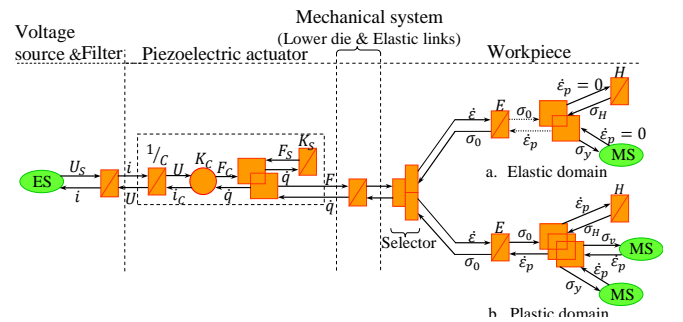


Fig. 6. Complete system's EMR

## IV. EXPERIMENT

### A. Experimental setup

Fig.7 shows the experimental equipment used for the test that will be compared to the simulation results. The specific elements of equipment are listed in table I. The test was carried out on a Lloyd LR30K material testing machine with a load capacity of 30 kN and a speed range of 0.001 to 508 mm/min.

TABLE I  
EXPERIMENTAL EQUIPMENTS

Displacement sensor	Heidenhain MT2581
Counter card	Heidenhain IK220
Force sensor	Kistler 9351B
Charge amplifier	Kistler 5015A
Current sensor	LEM
Voltage sensor	LEM
Piezoelectric actuator	Piezomechanik Pst1000/16/60
Acquisition card	NI 6124

The PA is powered by the current controlled by the Pulse Width Modulation (PMW) method at 3 kHz by using a voltage inverter connected in series with a filter. Since the two steel dies are assumed to be rigid, the relative displacements of the two workpiece surfaces are calculated from the displacements of the two dies, which are measured by displacement sensors. The force generated by the PA is measured by a force sensor between the lower die and the vibrating device. The measured signals of voltage, current and force are passed through a 4<sup>th</sup> order 1 kHz-anti-aliasing filter before being sampled by an acquisition card at 2 kHz, which is synchronised with the counter card that acquires the displacement measurements.

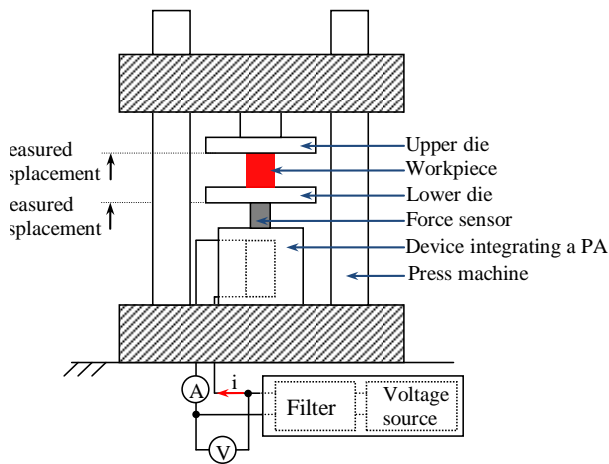


Fig. 7. Experimental setup

The vibrating device in Fig.8 is designed to ensure that the force applied to the PA (1) is only on its longitudinal axis. This aim is achieved by using a punctual contact (6) in order to transfer the vibrations from the PA to the plate (5), which is in contact with the force sensor. To create a linear slide for the punctual contact, a cylinder (2) is fastened to the plate. The movement of this cylinder is guided by the flexible linkages (4) connected to the outer fixed cylinder (3).

### B. Experimental results and discussion

The workpiece used in this experiment is an annealed copper cylindrical sample geometrically defined in table II. The material parameters provided in this table are identified and validated in other tests with different samples. These values were obtained through previous tests with various waveforms, but the identification procedure is beyond the scope of this paper. The Coulomb friction coefficient  $\mu$  is coarsely estimated. Indeed, a relatively short time at the

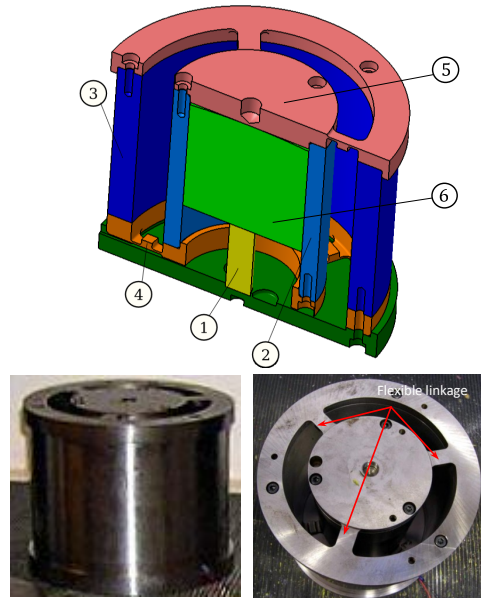


Fig. 8. Device integrating a PA

beginning of the test is considered for the identification. Therefore, the  $A$  term in Eq.10 is almost constant and difficult to identify.

TABLE II  
WORKPIECE'S PARAMETERS

$h$	7.9	[mm]
$r_e$	6	[mm]
$\sigma_y$	46.7	[MPa]
$E$	22.3	[GPa]
$H$	1.24	[MPa]
$\mu$	1	-
$\eta$	4.83	[GPa.s]
$n$	0.958	-
$m$	0.33	-

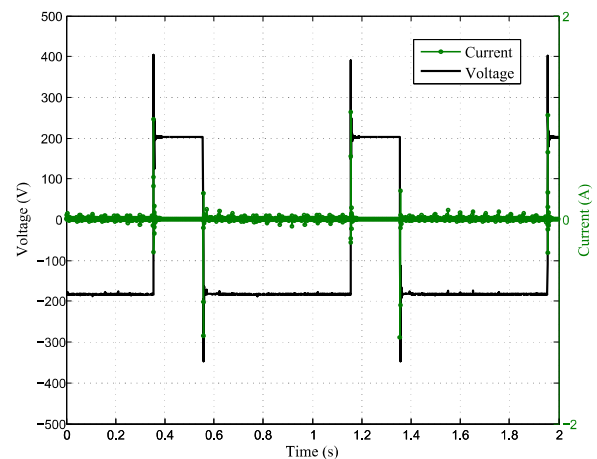


Fig. 9. Inverted output voltage and current in the PA

The voltage is a square wave of duty ration 10 % with the frequency 1.25 Hz. The peak to peak voltage is 400 V, and the bias voltage of 50 V is superimposed in order to respect the PA voltage rating. A pulsed current with a peak value of 1 A is thus applied to the PA (see Fig.9). The upper die moves down at a speed of 1 mm/min at  $t = 4$  s. The measured displacements and distance variations between the two dies

are presented in Fig.10. Results show that the machine is not rigid enough, and in the simulation, the displacement must be adjusted to obtain a displacement of ca. 4  $\mu\text{m}$ .

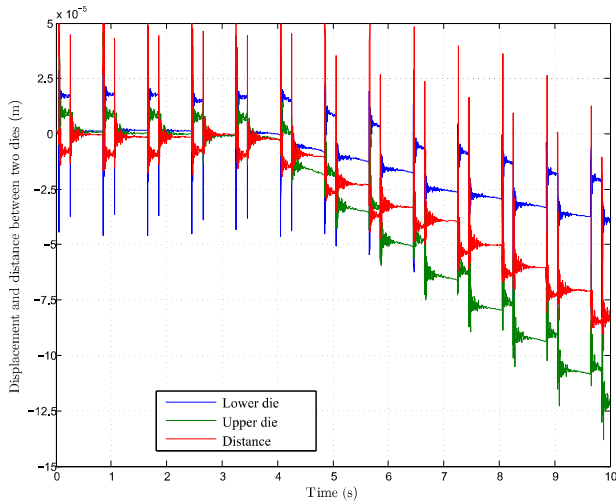


Fig. 10. Displacement and distance's variation between two dies

The measured forging load is compared with the simulated one in Fig.11. First, the simulated variations of the force are of the same magnitude as the measured ones (ca. 250 to 300 N depending on whether the beginning or the end of the curve is considered). However, the oscillations in the simulation are exaggerated, which could be a consequence of the value of  $\eta$  that was identified. As a matter of fact, the waveform used for the identification was triangular, and the speed involved was much lower. It can also be noticed that the initial elasto-plastic transition is a lot faster according to the model. This is known as the limitation of the Bingham model. The results at the end of the test present a departure of the predicted values from the actual ones. This separation can be attributed to the kinematic assumption of the slab model which ignores the barrelling effect common in the upsetting test.

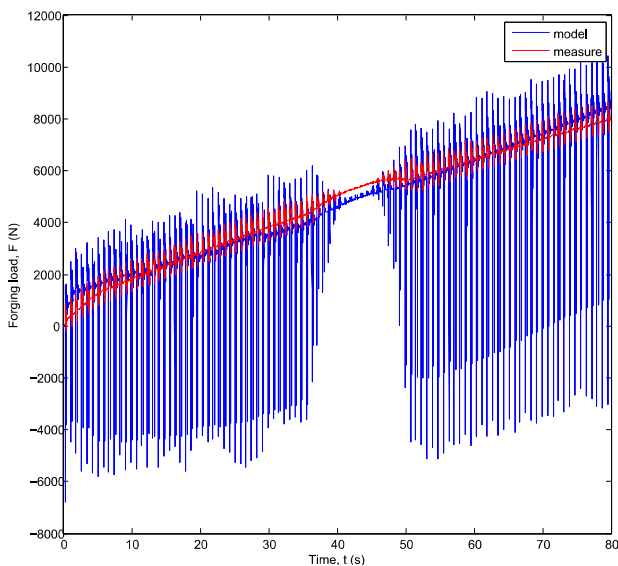


Fig. 11. Measured forging load in comparison with the simulated value

The results are nonetheless encouraging, in particular considering the details visible in Fig.12. The vibration is

suppressed around 38 s then put back around 46 s. In both cases this results in an increase of the forging load when the vibration is stopped, then a decrease of the forging load when the vibration is restored. This observation validates the model and the use of vibration. It also offers a practical way to study the influence of the waveforms and their parameters on reducing forging load in future works. Fig.13 gives an example of the influence of the change in waveform amplitude, period, and duty ratio (respectively 6  $\mu\text{m}$ , 50 ms and 40 %) on the forging force.

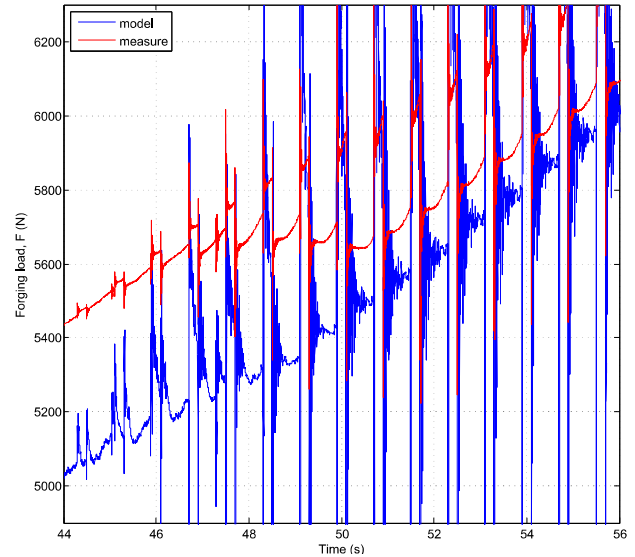


Fig. 12. Detail measured forging load in comparison with the simulated value

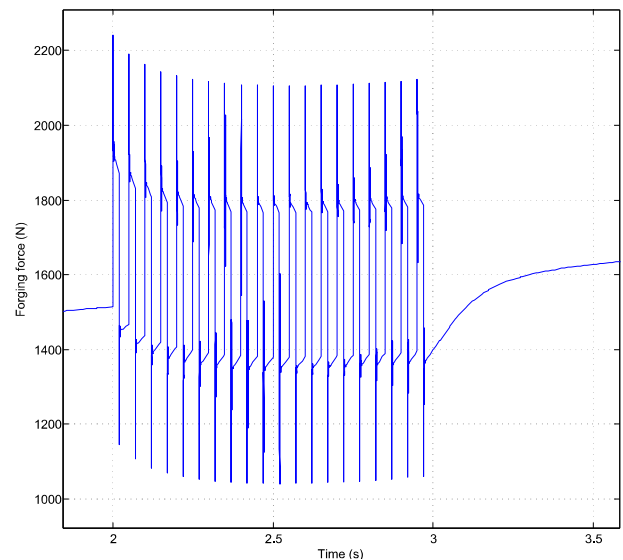


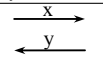
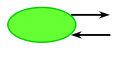
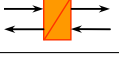
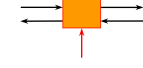
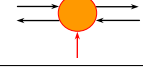
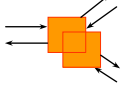
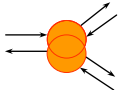
Fig. 13. Influence of waveform parameter change

## V. CONCLUSION

This work has proposed a model using Energetic Macroscopic Representation to predict the forging load during the forging process with the assistance of a piezoelectric stack actuator in low frequency. The EMR was used as a framework for building a sound model leading to a stable and fast simulation.

The confrontation of the model to experimental results reveals that the model seems to capture the main features of the process, which could facilitate the study of the impact of specific waveforms on forging force. The main limitation comes from the unexpected elasticity of the machine, which modifies the actual strains applied to the sample. Therefore, future work will focus on these problems and move to a larger test machine. According to the results obtained, the improvement of the model of the piezoelectric actuator will be addressed.

## VI. APPENDIX EMR's basic elements

Element	Symbol	Description
Variable		Action/ reaction variable ( $x/y$ )
Source		Energetic source
Accumulator		Accumulator
Converters		Mono-physic converter
		Multi-physic converter
Couplings		Mono-physic coupling
		Multi-physic coupling

## VII. ACKNOWLEDGEMENT

The authors would like to thank M. Fendler and Henrion for their technical support during the tests.

**Thanh Hung Nguyen** was born in Vietnam in 1983. He received his B.S. degree in Mechatronics from the Ho Chi Minh University of Technology, Vietnam, in 2006 and his M.S. degree from the École Nationale Supérieure de Mécanique et des Microtechniques de Besançon, France and the Hochschule Karlsruhe Technik und Wirtschaft, Germany in 2010. He is currently working towards the Ph.D degree at the École Nationale Supérieure d'Arts et Métiers, France. His research focuses on designing, modelling and controlling a system of multi-piezoelectric actuators to assist forging processes.

**Christophe Giraud-Audine** was born in Rabat (Morocco). He received his M.Eng. degree in mechanical engineering from the École Nationale Supérieure d'Arts et Métiers in 1992, and his Ph.D degree in electrical engineering from the Institut National Polytechnique de Toulouse in 1998. After two years spent as a Research Associate at the University of Sheffield, he joined an associate professor position at the École Nationale Supérieure d'Arts et Métiers. His current research focuses on the modelling and control of devices based on piezoelectric and shape memory alloys.

**Betty Lemaire-Semail** received her Ph. D degree in 1990 from the University of Paris XI, Orsay and habilitation degree in 1997 from the University of Lille 1. From 1990 to 1998, she was an assistant professor at the École Centrale of Lille and she is now a professor at the University of Lille 1. She is a member of the electrical engineering and power electronics laboratory of Lille (L2EP) and head of the research axis related to control of electrical systems. She has studied electromagnetic motors and her main field of interest now deals with the modelling and control of piezoelectric actuators for positioning and force feedback applications.

**Gabriel Abba** has joined the École Normale Supérieure de Cachan, France, in 1979, and received the "agrégation" of Ministry of Education in Electrical Engineering in 1982. He received the Doctorate degree in Electronics and Robotics from the University of Paris XI-Orsay, Paris, France, in 1986. Since 2004, he has been at The École Nationale d'Ingénieurs de Metz, where he is currently a Professor of Electrical and Computer Engineering. His research interests include development, modeling and control of robots, specially control of legged robots, visual servoing, manipulator control, design of robots and modelling and control of electromechanical actuators for industrial applications. He has made many contributions to robot dynamics and legged locomotion, and he has over 110 publications in Journals or Conferences.

**Régis Bigot** received his M.Eng. degree in mechanical engineering from the École Nationale Supérieure d'Arts et Métiers in 1992. In 1993 he obtained a master of sciences in Physics and Chemistry of Materials of University of Lille and his Ph.D degree in physical and metallurgy from the University of Lille in January 1996. After three years as technical teacher at Lille and Metz, he joined an associate professor position at the École Nationale Supérieure d'Arts et Métiers in September 1998. In September 2008, he becomes full professor in same institute. Since October 2011, he is director of Design, Manufacturing Engineering and Control Laboratory. His current research focuses on the manufacturing process (bulk forming, thixoforming, assembly, ...), integrated product and process design and CAPP.